J. Fluid Mech. (1977), *vol.* 80, *part* 4, *pp.* 685–703
Printed in Great Britain

Continuation or breakdown in tornado-like vortices

By ODUS R. BURGGRAF AND M. R. FOSTER

Department of Aeronautical and Astronautical Engineering,
The Ohio State University, Columbus

(Received 21 October 1975 and in revised form 18 July 1976)

Laboratory experiments on swirling flows through tubes often exhibit a phenomenon called vortex breakdown, in which a bubble of reversed flow forms on the axis of swirl. Mager has identified breakdown with a discontinuity in solutions of the quasi-cylindrical flow equations. In this study we define a tornado-like vortex as one for which the axial velocity falls to zero for sufficiently large radius, and seek to clarify the conditions under which the solution of the quasi-cylindrical flow equations can be continued indefinitely or breaks down at a finite height. Vortex breakdown occurs as a dynamical process. Hence latent-heat effects, though doubtless important to the overall structure and maintenance of the tornado, are neglected here on the scale of the breakdown process. The results show that breakdown occurs when the effective axial momentum flux (flow force) is less than a critical value; for higher values of the flow force, the solution continues indefinitely, with Long's (1962) similarity solution as the terminal state. When applied to the conditions of the 1957 Dallas tornado, the computed breakdown location is in agreement with Hoecker's analysis of the observations.

1. Introduction

In 1953, an interesting series of visual observations of tornadoes was made at close range by Reber, who published (in 1954) sketches of his observations together with related synoptic conditions. In several cases, a 'collar' or 'bulge' formed on the visible core of the tornado at a level of about 60% of the core height just before the funnel lifted from the ground. This feature is not necessarily representative of most tornado systems.† However, Ward (1972) has carried out some laboratory experiments in tornado modelling and he also observed a similar abrupt enlargement of the vortex-core diameter. He identified that condition with Reber's observations and also with a similar phenomenon previously noted in laboratory duct flows with swirl (Kirkpatrick 1964) and in leading-edge vortices of aircraft delta wings (Lambourne & Bryer 1961), viz. 'vortex breakdown'. Ward noted that breakdown in his experiments was associated with transition to turbulent flow, although other experimenters have obtained breakdown with a well-defined laminar bubble of reversed flow (Harvey 1962; Sarpkaya 1971).

Several theories have been put forward in the literature for the onset and structure of vortex breakdown. On the basis of an idea due to Squire (1960), Benjamin (1967)

† During part of its lifetime, the Jordan, Iowa tornado of 13 June 1976 developed such a bulge (see plate 1; private communication from Dr Robert Davis-Jones, NSSL).

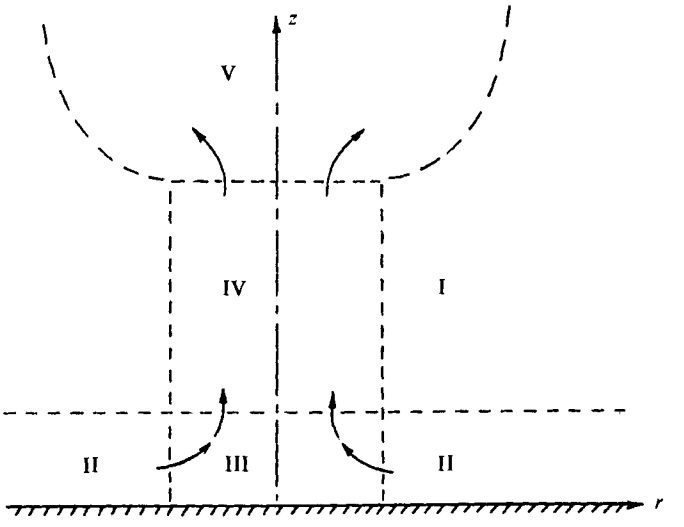

FIGURE 1. Cross-section of vortex showing regions of distinct types of flow (not to scale). I, potential vortex; II, boundary layer; III, eruption zone; IV, vortex core; V, reversed-flow bubble.

has developed a theory which likens vortex breakdown to a hydraulic jump. Hall (1972) critically reviewed this and earlier work, and presented some of his own numerical results as well. More recently, Mager (1972) has analysed the problem on the basis of momentum-integral theory, and found that vortex breakdown corresponds to a discontinuance of solutions of his equations. Randall & Leibovich (1973) theorized that vortex breakdown corresponds to a stationary-wave solution of the Korteweg–de Vries equation. Results from both these recent theories show trends in qualitative agreement with Sarpkaya's data.

Our idealization of the tornado corresponds to what Morton (1969) calls a 'vortex jet', i.e. a cylindrical structure which behaves like a potential vortex at the core edge and whose vertical velocity is large in the core but decreases to zero at the edge. This model may or may not be reasonable, since only sketchy information is available on velocity profiles in a tornado vortex. To date no theoretical work properly accounting for the viscous structure of the core has dealt with breakdown in a tornado-like vortex, although Barcilon (1967) has given an inviscid analysis of such a vortex.

The analysis presented herein is relevant as a fundamental flow problem in its own right, without reference to tornadoes. Certainly we have neglected some features of motion in the atmosphere, such as latent-heat release, baroclinic density variations and turbulence. It is not disputed that humidity is an essential ingredient in tornado formation and structure; the point here is that vortex breakdown is dynamical in character and that, on the scale of the breakdown process, latent-heat release would only obscure the fundamental mechanism involved. On a larger scale, of course, latent-heat effects must be included.

Referring to figure 1, the vortex jet is seen to be only a segment of the tornado flow field (this flow structure was proposed by Barcilon also). Region I is inviscid and the flow there consists of that due to a potential vortex. The boundary layer in region II delivers a certain amount of mass through the turning region (III) into the vortex core itself (IV). Region V is the region of reversed flow produced when

breakdown occurs. The parameter governing the structure of the vortex in region IV is the Reynolds number Γ/ν. If the Reynolds number is large, then the core is slender and the Navier–Stokes equations reduce to the set of equations which have come to be called the quasi-cylindrical equations (Hall 1966); for a homogeneous fluid, these are

$$\frac{\partial}{\partial r}(ru)+\frac{\partial}{\partial z}(rw)=0, \tag{1.1}$$

$$\partial P/\partial r = v^2/r, \tag{1.2}$$

$$u\frac{\partial}{\partial r}(rv)+w\frac{\partial}{\partial z}(rv)=\nu r\frac{\partial}{\partial r}\left(\frac{1}{r}\frac{\partial}{\partial r}(rv)\right), \tag{1.3}$$

$$u\frac{\partial w}{\partial r}+w\frac{\partial w}{\partial z}=\frac{\nu}{r}\frac{\partial}{\partial r}\left(r\frac{\partial w}{\partial r}\right)-\frac{\partial P}{\partial z}. \tag{1.4}$$

These equations are precisely those for a round jet except that the large swirl necessitates the retention of the centrifugal force, so that the pressure is *not* constant across the jet. The hydrostatic pressure is included in P, which represents the effective pressure $p/\rho+gz$.

The boundary conditions are

$$u = v = \partial v/\partial r = \partial w/\partial r = 0 \quad \text{on} \quad r = 0 \tag{1.5}$$

and

$$v \sim \Gamma/2\pi r, w \to 0 \quad \text{as} \quad r \to \infty. \tag{1.6}$$

At the base of region IV, $z = z_i$, one must specify (u, v, w), which are in principle determined by the structure of the flow leaving the eruption region III. In the absence of an adequate theory for region III, we shall assume initial conditions appropriate to laboratory experiments or natural observations. The radial velocity may *not* be specified independently: instead, as in boundary-layer theory, (1.1)–(1.4) may be used to obtain a differential equation for $u_i(r)$ in terms of $v_i(r)$ and $w_i(r)$, the azimuthal and vertical velocity components on $z = z_i$. The result is

$$\left[w_i w_i''+\frac{1}{r^2}w_i^2-\frac{1}{r}w_i w_i'-\frac{2v_i}{r^2}(rv_i)'\right]u_i-\frac{w_i^2}{r}(u_i'+ru_i'')$$
$$=\nu\left[w_i''' w_i+\frac{1}{r}w_i w_i''-\frac{1}{r^2}w_i w_i'-\frac{2}{r}v_i v_i''-\frac{2}{r^2}v_i v_i'+\frac{2}{r^3}v_i^2\right]. \tag{1.7}$$

If one integrates (1.4) across the core, the result is

$$\frac{d}{dz}\int_0^\infty r(P+w^2)\,dr = 0. \tag{1.8}$$

Hence, provided that the integral exists, it is invariant with z. Following Long (1962), we define the 'momentum transfer', also called the 'flow force', by the integral

$$J \equiv 2\pi\int_0^\infty r(P+w^2)\,dr, \tag{1.9}$$

and (1.8) requires that $dJ/dz = 0$. With condition (1.6) at the edge of the core, (1.2) indicates that as $r \to \infty$

$$P \sim P(\infty)-\Gamma^2/8\pi^2r^2.$$

Therefore, if J is to be bounded, the requirement is that

$$w \sim \Gamma/2^{\frac{3}{2}}\pi r \quad \text{as} \quad r \to \infty. \tag{1.10}$$

We have chosen for study the initial conditions

$$v_i = (\Gamma/2\pi r)\{1-\exp[-(r/\delta)^2]\}, \tag{1.11a}$$

$$w_i = \frac{\Gamma}{2^{\frac{3}{2}}\pi r}\{1-\exp[-(r/\delta)^2]\}^{\frac{1}{2}} + \left(w_0 - \frac{\Gamma}{2^{\frac{3}{2}}\pi\delta}\right)\exp[-(r/\delta)^2], \tag{1.11b}$$

where w_i clearly decays exponentially to the form (1.10), and $w_i = w_0$ on the axis. δ is a characteristic width of the vortex profile, and the parameter $2\pi w_0\,\delta/\Gamma \equiv \alpha$ totally characterizes the structure of $\delta w_i/\Gamma$. Solutions of (1.1)–(1.4) with these initial conditions must then have the property of constant flow force.

The question of chief interest here is simply stated: for what values of α (or equivalently J/Γ^2) will conditions (1.11) lead to a smoothly flowing vortex jet as $z\to\infty$, and, conversely, for what (if any) values of α will the solution break down at some finite $z = z^*$? Self-similar vortex-jet solutions satisfying edge boundary condition (1.10) have been found by Long (1962), and we propose that they are related to a large-z solution of (1.1)–(1.4) when one exists. In § 2 we discuss these similarity solutions in detail, improved results having been obtained by a shooting technique. The similarity solution is taken as the first term of the asymptotic solution of (1.1)–(1.4) in inverse powers of z and the next term is considered in § 3. We show numerical solutions of (1.1)–(1.4) with boundary conditions (1.5), (1.6) and (1.10) and initial conditions (1.11) in § 4, and some details of the structure of the breakdown region when it occurs.

2. Improved solutions of similarity equations

The relevance of Long's (1962) similarity solutions to the terminal state of the vortex jet is anticipated here, and pertinent properties of these solutions are examined. The essential nature of Long's solution is contained in his similarity variable

$$y = Kr/2^{\frac{1}{2}}\nu z, \tag{2.1}$$

where $K = \Gamma/2\pi$ is a circulation parameter and ν is the kinematic viscosity of the fluid. Clearly, surfaces of constant y are cones with apex at the origin. It can be shown that (2.1) is the only similarity variable of the form r/z^n that permits solutions of the governing equations (1.1)–(1.4).

In terms of a stream function ψ, the radial and axial components of the velocity are defined as

$$u = -r^{-1}\,\partial\psi/\partial z, \quad w = r^{-1}\,\partial\psi/\partial r.$$

In similarity form the flow variables are given as follows. For the meridional flow,

$$\psi = \nu z f_0(y), \tag{2.2}$$

$$w = (K/2^{\frac{1}{2}}r)f_0'(y), \tag{2.3}$$

$$u = (-\nu/r)f_0(y) + (K/2^{\frac{1}{2}}z)f_0'(y), \tag{2.4}$$

for the azimuthal flow,

$$v = (K/r)\,g_0(y), \tag{2.5}$$

and for the pressure,

$$P = (-K^4/\nu^2 z^2)\,s_0(y). \tag{2.6}$$

In terms of these similarity variables the governing equations (1.1)–(1.4) reduce to the set of ordinary differential equations first given by Long:

$$2y^3 s_0' + g_0^2 = 0, \tag{2.7}$$

$$y g_0'' - (1 - f_0) g_0' = 0, \tag{2.8}$$

$$y f_0'' - (1 - f_0) f_0' - 4y^3 s_0 = 0. \tag{2.9}$$

Note that (2.9) is a first integral of (1.4). Corresponding to (1.9), we define

$$m = \pi \int_0^y [-4y^2 s_0(y) + f_0'^2(y)] \frac{dy}{y}.$$

Thus to the set (2.7)–(2.9), we add the differential equation

$$y m' + 4\pi y^2 s_0 - \pi f_0'^2 = 0 \tag{2.10}$$

and note that the non-dimensional flow force is given by

$$m(\infty) = J/K^2 \equiv M. \tag{2.11}$$

For boundary conditions on (2.7)–(2.10), rewrite (1.6) and (1.10) in similarity variables:

$$f_0'(\infty) = g_0(\infty) = 1. \tag{2.12}$$

The method of solution of (2.7)–(2.10) was by an iterative–shooting technique (Nachtscheim & Swigert 1965), but with several refinements over the numerical solutions of the same equations previously obtained by Long (1962). It may be shown from (2.8) that g_0 approaches its asymptotic value of 1 exponentially. Thus (2.7) shows that

$$s_0 \sim 1/4y^2 \quad \text{as} \quad y \to \infty \tag{2.13}$$

and (2.9) indicates that

$$f_0' \sim 1 - \frac{\alpha}{y^2} - \frac{4\alpha}{y^3} - \frac{3(12-\alpha)\alpha}{2y^4} + \ldots \quad \text{as} \quad y \to \infty, \tag{2.14}$$

so that s_0 and f_0' both approach their edge values only algebraically. In the numerical solution, (2.13) and (2.14) were used to correct for slow decay to the asymptotes, since α may be determined from

$$\alpha = \lim_{y \to \infty} y^2 (1 - f_0').$$

Further, the flow force M approaches its value slowly as the edge is taken to infinity; i.e., from (2.10) and (2.14),

$$M - m(y) \sim -\pi\alpha/y \quad \text{as} \quad y \to \infty. \tag{2.15}$$

We also corrected the computed value of the flow force using (2.15). More details of the numerical method may be found in Burggraf & Foster (1975).

The properties of the solutions so obtained were described by Long, and include the remarkable feature of non-uniqueness: any given value of M corresponds to two different solutions. However, the results given by Long do not allow ready comparison of the solution pair for a given M, nor is M given to any useful accuracy. Our interest is in possible terminal states of the vortex jet for the M corresponding to our assumed

M	a_0	α
3·75	0·0488	−3·915
	0·0284	−4·31
3·8	0·0839	−3·389
	0·0165	−4·99
4·0	0·1501	−2·707
	−0·0307	−6·327
5·0	0·3520	−1·611
	−0·0675	−11·189
6·0	0·5155	−1·138
	−0·0711	−16·377

TABLE 1. Parameter values for self-similar vortex jets.

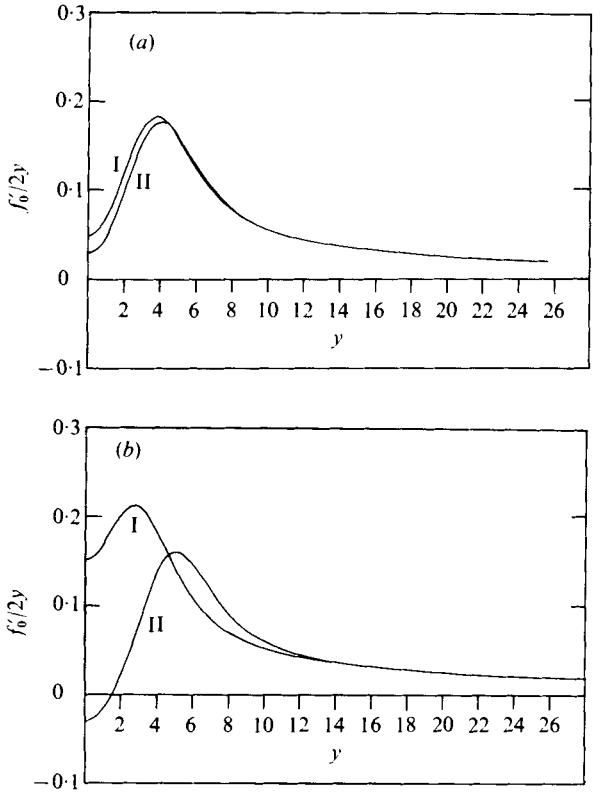

FIGURES 2(*a*, *b*). For legend see next page.

initial state (1.11). Hence it was deemed essential to carry out accurate solutions with the emphasis on selected values of M.

We define $a_0 = w(0)\nu z/K^2$. Table 1 gives pairs of values of a_0 and the parameter α appearing in the asymptotic formulae for large y. This table illustrates the following properties of the solutions:

(i) The minimum value of M for which a solution can be found is very nearly 3·75, compared with the value of 3·65 given by Long (1962). We denote this value by M^*.

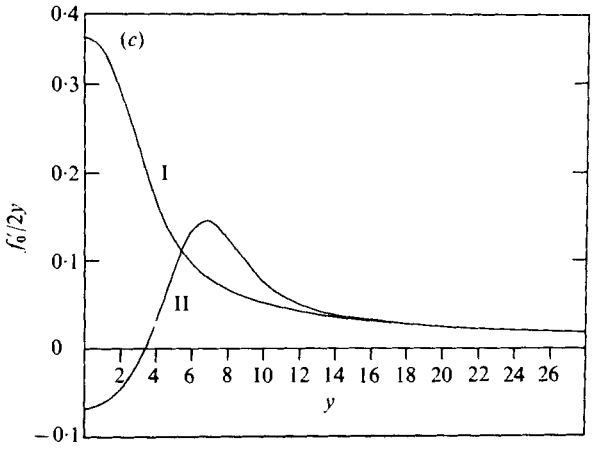

FIGURE 2. Similarity solution: vertical velocity profiles.
(*a*) $M = 3{\cdot}75$, (*b*) $M = 4{\cdot}0$, (*c*) $M = 5{\cdot}0$.

(ii) For $M < 4{\cdot}71$, both members of the solution pair for a given M exhibit a defect of axial velocity in the vicinity of the axis.

(iii) For $M > 3{\cdot}81$, one member of the solution pair has flow reversal at the axis ($a_0 < 0$). These reversed-flow solutions may have relevance to the current belief that the flow at the centre of a tornado is downward.

Vertical velocity profiles are shown in figure 2 for $M = 3{\cdot}75$, $4{\cdot}0$ and $5{\cdot}0$. The solution pair for $M = 3{\cdot}75$ closely brackets the unique solution for the minimum M. Both exhibit severe velocity defects on the axis, although the velocity on the axis is positive for both. For $M = 4$, the velocity defect is less severe for one solution, but has deepened for the other to the point of reversing the flow on the axis. For $M = 5$, the defect is no longer present in one solution, while the core of flow reversal has grown larger in the other. The critical value of M at which the velocity defect just disappears is $4{\cdot}71$.

For convenience in later discussion, we call the solution with the smaller axial velocity defect (i.e. the algebraically larger value of a_0) a type I solution, and the other a type II solution. Hence the solutions exhibiting flow reversal are all of type II. This notation is employed in figures 2 and 3.

Solution curves for the swirl velocity v and pressure P for $M = 4{\cdot}0$ are shown in figure 3. The width of these profiles is rather less than that of the axial velocity profiles, corresponding to exponential decay of v and P to their external potential-vortex behaviour, in contrast to the algebraic decay of w. Further discussion of the similarity solutions will be given in § 4, where they are compared with flows developing from non-similar initial states.

3. Perturbation of similarity solution

As stated previously we expect the similarity solution of § 2 to represent the large-z structure of a vortex jet with finite flow force. An important question in regard to detailed comparison of such a self-similar solution with the solutions obtained by marching (see § 4) is the deviation of the numerical solution from the similar solution

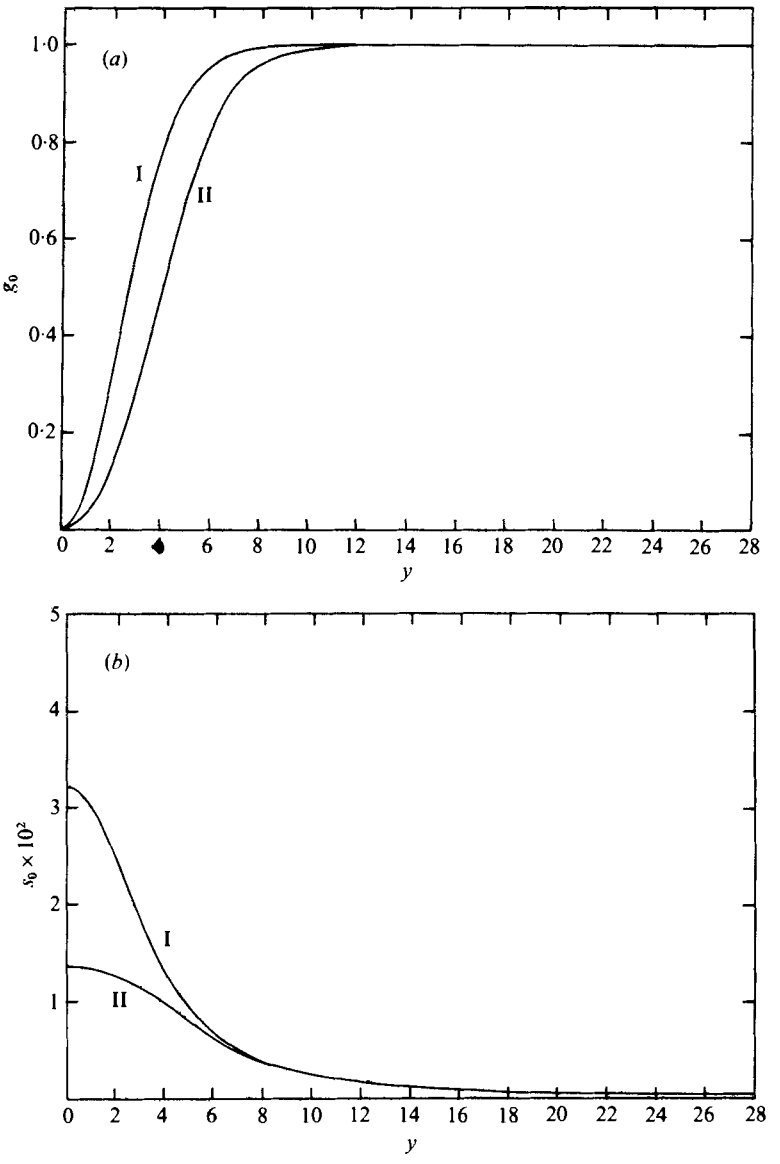

FIGURE 3. Similarity solution for $M = 4{\cdot}0$. (*a*) Angular momentum profiles. (*b*) Pressure profiles.

for large but finite z. The quasi-cylindrical equations (1.1)–(1.4) have the following asymptotic expansion for large z:

$$\left.\begin{aligned} \psi &= \nu z[f_0(y) + (l/z) f_1(y) + \ldots], \\ v &= (K/r)\,[g_0(y) + (l/z)\, g_1(y) + \ldots], \\ P &= (-K^4/\nu^2 z^2)\,[s_0(y) + (l/z)\, s_1(y) + \ldots], \end{aligned}\right\} \tag{3.1}$$

where y is the similarity variable of (2.1) and l is a characteristic length associated with upstream conditions. The zero subscripts denote Long's self-similar solution of § 2.

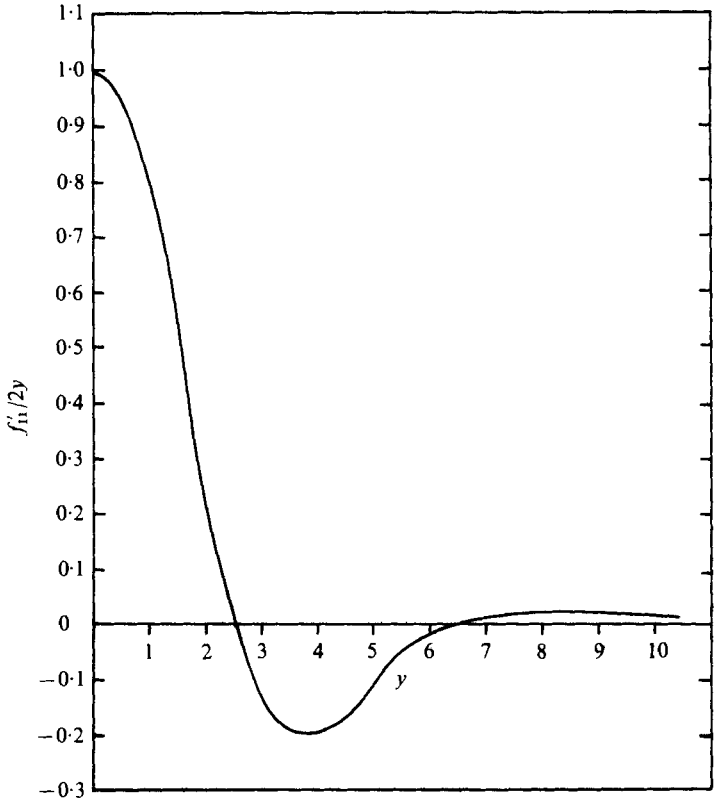

FIGURE 4. Axial velocity perturbation solution for zero swirl perturbation.

When (3.1) is substituted into (1.1)–(1.4), the zero-order terms give Long's equations (2.7)–(2.9), while the terms of next higher order yield

$$y^3 s_1' + g_0 g_1 = 0, \tag{3.2}$$

$$y g_1'' - (1 - f_0) g_1' + f_0' g_1 = 0, \tag{3.3}$$

$$y^2 f_1''' - (1 - f_0) y f_1'' + (1 + f_0 + 3y f_0') f_1' - 4y(y^3 s_1)' = 0. \tag{3.4}$$

Two types of solution of (3.2)–(3.4) have been identified. The first type simply represents an origin shift of the zero-order solution. A solution of this type is to be expected, since the virtual origin of the similarity solution need not be at $z = 0$. Suppose that we shift the origin through a distance Δz, replacing z wherever it occurs in (2.2) by $z + \Delta z$. On expansion for small Δz, such a procedure gives a perturbation of the similarity solution with l in (3.1) equal to Δz. We denote this origin-shift solution by adding a second subscript zero. Thus

$$f_{10}(y) = f_0(y) - y f_0'(y), \tag{3.5}$$

$$g_{10}(y) = -y g_0'(y), \tag{3.6}$$

$$s_{10}(y) = -2 s_0(y) - y s_0'(y). \tag{3.7}$$

The second type of solution of (3.2)–(3.4), which we now denote as (f_{11}, g_{11}, s_{11}), has no such simple physical interpretation. Being motivated by the non-similar marching solutions discussed in § 4, we seek perturbations in the axial flow that are not coupled with the swirl flow. In that case, g_{11} and s_{11} both vanish, and f_{11} is given by the reduced form of (3.4):

$$y^2 f_1''' - y(1-f_0)f_1'' + [(1+f_0) + 3yf_0']f_1' = 0. \tag{3.8}$$

From (3.8) it can be shown that the asymptotic form of f_{11}' decays either algebraically like y^{-2} or exponentially like $\exp(-y)$. The algebraic decay term dominates and, after some algebra, we find several terms in the asymptotic expansion for large y:

$$f_{11}' \sim \frac{\beta}{y^2} + \frac{6\beta}{y^3} + \frac{3\beta}{y^4}(12-\alpha) + \ldots, \tag{3.9}$$

where α is defined in § 2. Numerical solutions of (3.2)–(3.4) were obtained by a shooting method as in § 2 using the asymptotic structure given above.

The velocity profile $f_{11}'(y)/2y$, proportional to w_{11}, is shown in figure 4. We observe that this type of perturbation mainly affects the flow quite near the axis. The sign change noted near $y = 2{\cdot}5$ is required by the condition that the flow force be unchanged by the perturbation.

The first-order perturbation of M is given by

$$\Delta M = \int_0^\infty (f_0' f_1' - 2y^2 s_1)\frac{dy}{y},$$

and, since $s_1 \equiv 0$ for this case, and $f_0' > 0$ for all y, it is clear that f_{11}' must change sign to make ΔM vanish.

4. Marching solutions

4.1. *The numerical method*

To recapitulate, the numerical problem under consideration in this section is to solve (1.1)–(1.4) subject to boundary conditions (1.5) and (1.6) with the aim of determining whether or not the solutions continue to arbitrarily large z or break down, and of determining the nature of the terminal state in either case. The numerical scheme selected is a modification of one used earlier by Burggraf, Stewartson & Belcher (1971) to study the boundary layer induced by a potential vortex. A similar scheme was used by Hall (1967) to calculate several examples of vortex breakdown, such as swirling flow through tubes and leading-edge vortices on delta wings.

For an arbitrary variable $\phi(r, z)$, define the quantities ϕ_j, ϕ_j' and $\overline{\phi}_j$ as

$$\phi_j = \phi(r_j, z_i), \quad \phi_j' = \phi(r_j, z_{i+1}), \quad \overline{\phi}_j = \tfrac{1}{2}(\phi_j + \phi_j'),$$

where $z_{i+1} = z_i + \Delta z$ and $r_{j\pm1} = r_j \pm \Delta r$. Derivatives are then defined in the usual manner as

$$\partial\phi/\partial z = (\phi_j' - \phi_j)/\Delta z, \quad \partial\phi/\partial r = (\overline{\phi}_{j+1} - \overline{\phi}_{j-1})/2\Delta r,$$

$$\partial^2\phi/\partial r^2 = (\overline{\phi}_{j+1} - 2\overline{\phi}_j + \overline{\phi}_{j-1})/(\Delta r)^2.$$

Thus the equations of motion (1.1)–(1.4) are replaced by a finite-difference analogue, which can be expressed in matrix notation as

$$\mathbf{T}_1\mathbf{V} = \mathbf{R}, \quad \mathbf{T}_2\mathbf{W} = \mathbf{S}. \tag{4.1}$$

Here $\mathbf{T}$ is a tridiagonal square matrix whose elements depend on z_i, r_j, $\overline{w}_j$ and $\overline{u}_j$, $\mathbf{V}$ and $\mathbf{W}$ are column vectors representing the v_j and the w_j respectively and $\mathbf{R}$ and $\mathbf{S}$ are column vectors for (1.3) and (1.4) whose elements are known functions of the flow properties at (r_j, z_i) as well as the unknown properties at (r_j, z_{i+1}).

The fact that $\mathbf{T}$ is tridiagonal permits a highly efficient solution algorithm, based on the Gauss-reduction procedure. Only the non-vanishing matrix elements on the three diagonals are stored. The elements on the subdiagonal can be reduced to zero successively; the equations can then be solved one after another, starting at the bottom of the matrix. This procedure requires of the order of $6N$ multiplications and divisions for the complete solution, compared with order N^3 for conventional methods. The nonlinearity of the problem manifests itself in the fact that the elements of $\mathbf{T}$ depend on the solution for $\mathbf{V}$ and $\mathbf{W}$. Hence the solution procedure is iterated at a given station until the desired degree of convergence is attained. The convergence criterion chosen was usually a repetition of the solution vectors to within 10^{-5} for single-precision computations or 10^{-7} for double-precision.† Depending on the z step chosen, typically 10–20 iterations were required for convergence.

Both cylindrical-polar and spherical-polar co-ordinates were used, the latter having been thought to be more appropriate to the development of a terminal similarity solution. However, experience showed that even in that case proper use of cylindrical-polar co-ordinates gave more accurate solutions, as judged by the smallness of variation of the flow force with z. In that case, the maximum mesh radius for cylindrical co-ordinates must be increased at regular intervals. This was accomplished automatically in these calculations by increasing the overall mesh radius by a fixed amount (20 additional mesh points) whenever the axial velocity deviated from boundary condition (1.10) by more than a specified tolerance (say, 5×10^{-4}) at any of the three outermost interior mesh points. When breakdown occurred, the mesh radius grew at an increasingly rapid rate as the critical point was approached. In other cases, the mesh radius tended towards a constant growth rate, indicative of the conical growth of self-similar vortex jets.

The complete vortex-jet solutions were obtained by a marching procedure, starting with the initial profiles for $v_i(r)$ and $w_i(r)$ given by (1.11) with $u_i(r)$ determined from (1.7). We arbitrarily set $z = 0$ at this station, and then march forward in z, solving the system (4.1) at each z step as we go. Because the system of equations (1.1)–(1.4) is of parabolic type, the marching procedure will continue as long as $w > 0$ everywhere (the decay to zero for $r \to \infty$ is not significant for $w \sim 1/r$). However, if a z station is reached at which $w \leqslant 0$, the solution procedure breaks down.‡ On physical grounds, this breakdown of the solution when w changes sign should be expected, since the streamlines on which $w < 0$ carry backwards information concerning unspecified conditions at larger z. The question of whether the solution will break down or continue

† All programmed computations in this study were carried out on an IBM 370-165 digital computer.

‡ Numerically breakdown occurs while w is still positive; the axial gradient of w becomes so large that the iteration procedure fails to converge even for very small values of Δz.

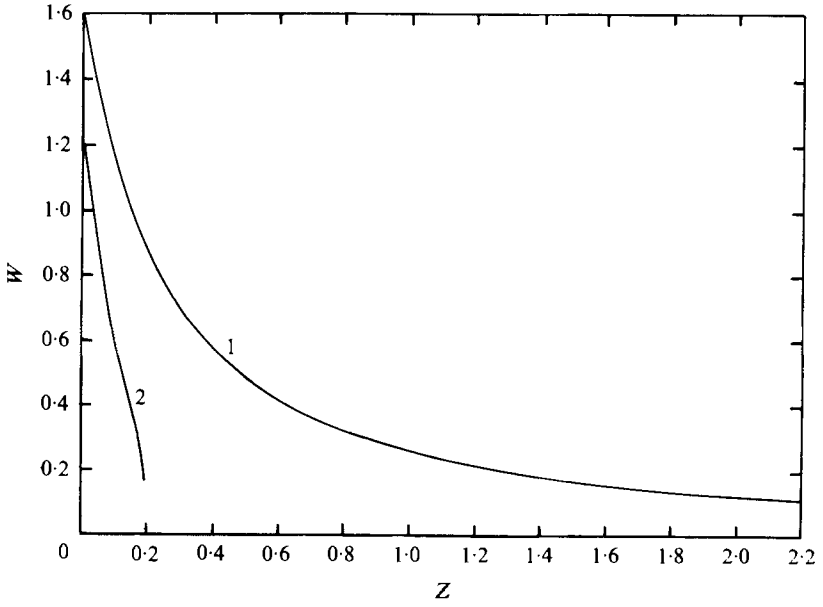

FIGURE 5. Axis speed from the marching solutions for (1) $M = 4{\cdot}0$ and (2) $M = 1{\cdot}7$.

indefinitely can thus be recast as whether or not the axial velocity vanishes at a finite height. The answer to this question depends on the value of the flow force J relative to the circulation Γ, as will be seen from the numerical results discussed below.

4.2. *Numerical results*

By the methods described above, (1.1)–(1.4) were integrated in z subject to edge conditions (1.6) and (1.10) and with profiles on $z = z_i$ given by (1.11). Defining M as J/K^2 from (1.9), we found the following.

(i) If $M > M^*$, integration in z may be continued arbitrarily far and the solution as $z \to \infty$ approaches the similarity solution of § 2.

(ii) If $M < M^*$, the vortex jet terminates with $w(0) \to 0$ at a finite z (say z^*), apparently signalling the onset of an axisymmetric reversed-flow bubble, characteristic of one sort of vortex breakdown.

The critical value M^* of the flow force, i.e. the value of M below which no similarity solutions exist (see § 2), is about 3·75. Hence the role of the similarity solution of type I (in the terminology of § 2) is that, when such a similarity solution exists, it is the terminal state of such a vortex jet; when similarity does *not* exist ($M < M^*$), the vortex jet undergoes vortex breakdown at z^*. For convenience in the following discussion, we use non-dimensional variables $R \equiv r/\delta$, $Z \equiv \nu z/K\delta$, $U = u\delta/\nu$, $V = v\delta/K$ and $W = w\delta/K$. Figure 5 shows W on the vortex axis *vs.* Z for two different values of M, one above and one below M^*. Note that for the case $M = 1{\cdot}70$ we extrapolate to find $Z^* = 0{\cdot}202$.

We describe in detail below the two particular cases shown in figure 5; we shall refer to the solution with $M = 4$ as case 1 and to that with $M = 1{\cdot}7$ as case 2. A variety of mesh sizes were used to study the effects of truncation error on the numerical results. The values for ΔR and ΔZ given in specific cases below represent those found

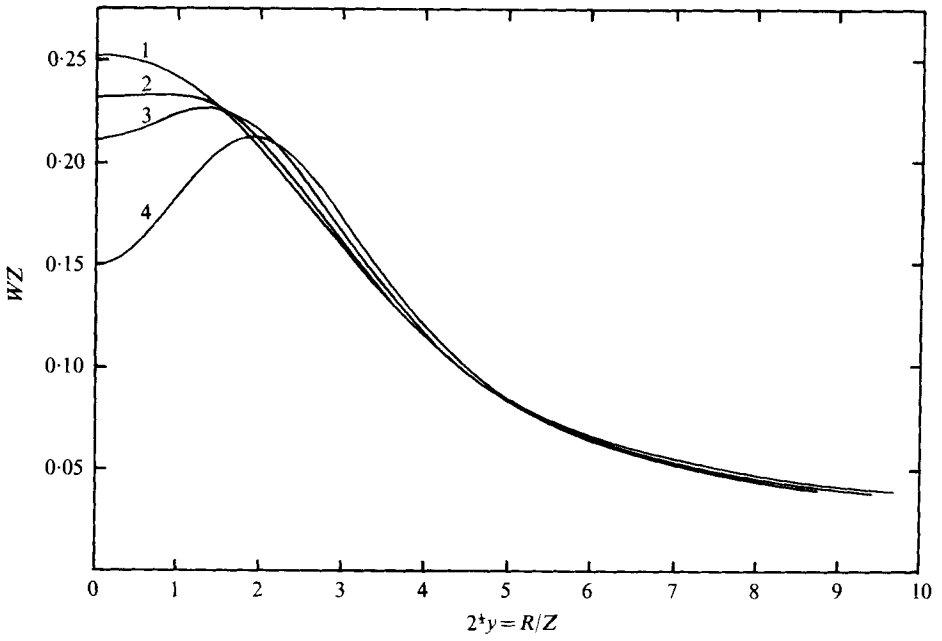

FIGURE 6. Vertical velocity profiles from the marching solution for $M = 4{\cdot}0$, plotted in similarity variables. (1) $Z = 2{\cdot}04$. (2) $Z = 4{\cdot}01$. (3) $Z = 8{\cdot}00$. (4) Similarity solution.

to give acceptable accuracy while keeping machine time to a reasonable length. We obtained both single- and double-precision results to determine the effects of round-off errors, which are especially significant in cases where breakdown occurs.

As stated in § 1, the flow force M must be constant with z, so we computed M at every z station to check that invariance. Since w decays algebraically and not exponentially to its edge value of $K/2^{\frac{1}{2}}r$, the tail of the w profile beyond the finite edge location adds a small contribution to the integral for M. This effect plus some truncation error seem to explain the fact that our calculated M decreases slowly with Z in the numerical integration. In case 1, M decreases from the starting value of 4·01 to 3·85 at $Z = 8{\cdot}00$; for case 2, M decreases from 1·70 to 1·64 from $Z = 0$ to $Z = 0{\cdot}196$. Using a two-term asymptotic expansion for M [see (2.15)], we can compute the contribution to M from the neglected tail of the w profile at $Z = 8{\cdot}00$, assuming that it is nearly similar; such a calculation gives a ΔM of 0·067 for that case, which is about 40 % of the observed decrease. Truncation error due to $\Delta R > 0$ probably accounts for the remainder. The results given for case 1 in this section are single-precision. The effects of round-off errors were shown to be negligible by repeating the calculation in double precision to $Z = 4{\cdot}84$, with very minor changes in the results.

In case 1, for the results given below we used $\Delta R = 0{\cdot}125$ with $\Delta Z = 0{\cdot}0008$ for $Z < 0{\cdot}0408$ and $\Delta Z = 0{\cdot}004$ for $Z > 0{\cdot}0408$. The calculation proceeded from $Z = 0$, where there were 200 radial points, to $Z = 8{\cdot}00028$, where 1121 points were necessary; the algorithm used to allow vortex growth with Z has been discussed in § 4.1. For case 2, we used $\Delta Z = 0{\cdot}002$ and $\Delta R = 0{\cdot}05$, with 200 radial mesh points at $Z = 0$ and 380 points near breakdown; the results given below for this case were computed in double precision. The vortex grows very rapidly as $z \to z^*$.

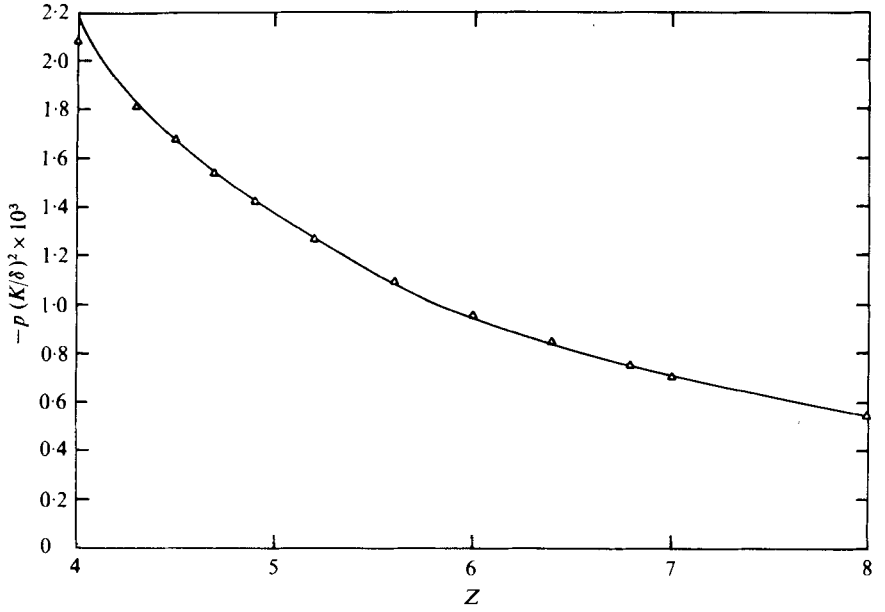

FIGURE 7. Comparison of axis pressure from the marching solution (triangles) with the two-term asymptotic solution (solid line) with $\Delta Z = -0{\cdot}341$ [see (4.4*b*)]. $M = 4{\cdot}0$.

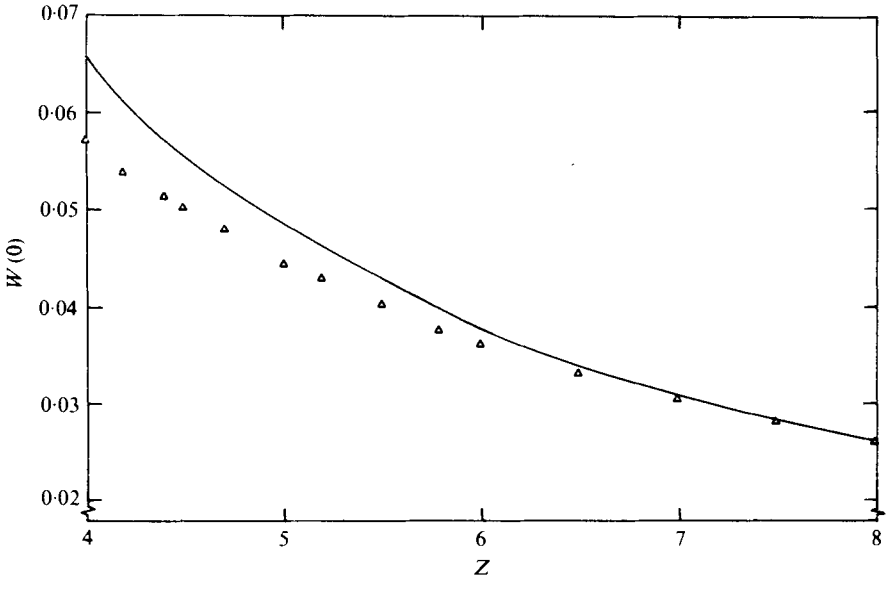

FIGURE 8. Comparison of axis speed from the marching solution (triangles) with the two-term asymptotic solution (solid line) with $\Delta Z = -0{\cdot}341$, $L = 4{\cdot}59$ [see (4.4*a*)]. $M = 4{\cdot}0$.

In case 1, for $M = 4{\cdot}01 > M^*$, a few of the vertical velocity profiles at various z stations are shown in figure 6 *vs.* the similarity variable of § 2. For values of Z beyond about 4, a velocity defect develops on the axis. The self-similar solution for this value of M (figure 2*b*) also shows such a defect and is plotted in figure 6 for comparison. In similarity variables, the hypothesis of approach to similarity appears to be borne out.

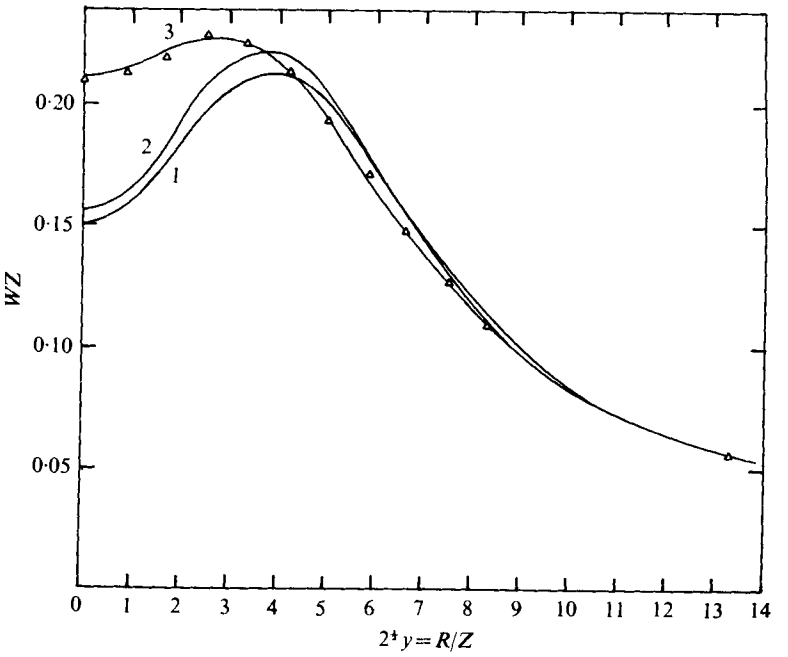

FIGURE 9. Comparison of the axial velocity profiles for $M = 4{\cdot}0$ from the marching solution and the two-term asymptotic solution. (1) Similarity solution. (2) Similarity solution with origin shift, $\Delta Z = -0{\cdot}341$. (3) Equation (4.5) with $\Delta Z = -0{\cdot}341$, $L = 4{\cdot}59$. $\triangle$, marching solution at $Z = 8{\cdot}00$.

Numerically, of course, one cannot achieve exact similarity since $z = \infty$ is unattainable; an additional difficulty for this case is that the decay to the similarity state is quite slow; for large M the rate of approach to similarity would be faster. However, the case M near M^* was chosen because it provides a more critical test of the hypothesis that the similarity solution is the terminal state.

Consider the conditions on the axis for large z. From (3.1), we know that as $z \to \infty$

$$[\nu z w/K^2]_{r=0} \sim \tfrac{1}{2}f_0''(0) + \tfrac{1}{2}(l/z)f_1''(0) + \ldots, \tag{4.2a}$$

$$[-\nu^2 z^2 P/K^4]_{r=0} \sim s_0(0) + (l/z)\,s_1(0) + \ldots. \tag{4.2b}$$

For that portion of (f_1, s_1, g_1) associated with an origin shift Δz, (3.5) and (3.7) indicate that

$$f_{10}''(0) = -f_0''(0), \quad s_{10}(0) = -2s_0(0). \tag{4.3a,b}$$

Further, there is a part of $f_1''(0)$ due to the solution f_{11}, so we write the velocity and pressure on the axis as

$$2[\nu z w/K^2]_{r=0} \sim f_0''(0)\,(1 - \Delta Z/Z) + (L/Z)f_{11}''(0) + \ldots, \tag{4.4a}$$

$$[-\nu^2 z^2 P/K^4]_{r=0} \sim s_0(0)\,(1 - 2\Delta Z/Z + \ldots), \tag{4.4b}$$

where L represents some length scale associated with the non-similar nature of the initial profile w_i. Equation (4.4b) is plotted in figure 7 together with the numerical solution for $M = 4$. If one chooses a virtual origin such that $\Delta Z = -0{\cdot}341$, we see that the agreement is quite good. A similar result would hold for v, since pressure is simply

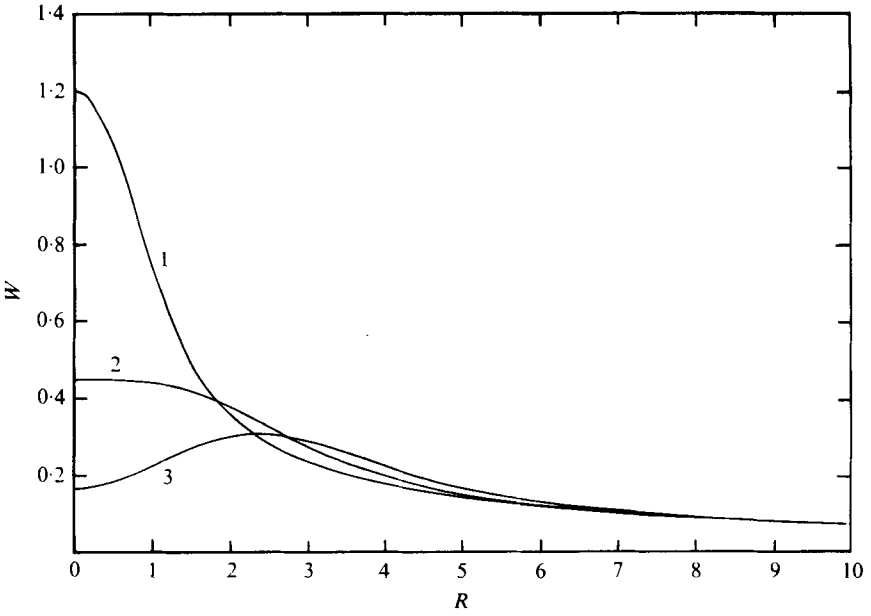

FIGURE 10. Vertical velocity profiles from the marching solution for $M = 1{\cdot}7$. (1) $Z = 0$; (2) $Z = 0{\cdot}138$; (3) $Z = 0{\cdot}196$.

an integral of the azimuthal velocity and the numerical results indicate that by $Z = 6$ the azimuthal velocity is self-similar. A similar comparison of (4.4a) with the numerical solution yields poor agreement if $L \equiv 0$; however, including f'_{11} with $L = 4{\cdot}59$ gives very good agreement at Z near 8 between the asymptotic result and the numerical solution for the axis velocity, as shown in figure 8. The comparison is made more convincing by considering the full velocity profile. Equations (3.1) and (3.5) combine to give the following two-term expansion for $Z \to \infty$:

$$\frac{w\delta}{K} = \frac{1}{2Z}\left(\frac{f'_0(y)}{y} - \frac{\Delta Z}{Z} f''_0(y) + \frac{L}{Z}\frac{f'_{11}(y)}{y}\right). \tag{4.5}$$

In figure 9, we plot the similarity solution for $M = 4$, the part of (4.5) including origin shift only ($\Delta Z = -0{\cdot}341$, $L \equiv 0$), and (4.13) with $\Delta Z = -0{\cdot}341$, $L = 4{\cdot}59$. We also include in figure 9 the marching solution described above for $M = 4$. The agreement of the W profile from the asymptotic solution with that from the marching solution clearly supports our hypothesis that the similarity solutions of § 2 are large-z asymptotic solutions of the quasi-cylindrical equations for $M > M^*$.

Returning now to case 2 above ($M = 1{\cdot}7 < M^*$), vortex breakdown occurs here at $Z^* = 0{\cdot}202$. The velocity on the axis in this case drops precipitously as may be seen in figure 5. Figure 10 shows vertical velocity profiles for this case. Note that a velocity defect occurs very rapidly (as compared with the case $M = 4{\cdot}0$ in figure 9). The details of the structure of the solution at z near z^* are interesting, though a detailed analytical structure has yet to be worked out. An indication of the structure can be found from the numerical solution at the last converged z station ($Z = 0{\cdot}196$), by comparing the magnitudes of terms in the partial differential equations (1.3) and (1.4). The details of such comparisons may be found in Burggraf & Foster (1975), but the numerical

results show quite clearly that viscous diffusion is negligible except possibly at great distances from the vortex axis. The conclusion is that the rapid spreading of the vortex just upstream of breakdown is an inviscid phenomenon, perhaps not unlike the inviscid turning of a jet impinging on a wall.†

The equations in the breakdown region then appear to be the inviscid, Euler equations in the axial and azimuthal directions, which have solution

$$rv = G(\psi), \quad P + \tfrac{1}{2}(v^2 + w^2) = F(\psi), \tag{4.6}$$

with

$$ru = -\partial\psi/\partial z, \quad rw = \partial\psi/\partial r.$$

In addition, the radial force balance is

$$\partial P/\partial r = v^2/r. \tag{4.7}$$

The unknown functions F and G are determined by the upstream solution, i.e. the numerical solution for $z - z^* \to 0$. Further details of such an analysis are left for future work.

5. Discussion

A number of earlier studies have dealt with vortex breakdown; these however have been concerned with vortex flows in which the external conditions correspond to flow in a duct or past an aircraft wing. The present calculation of the development of a vortex jet appears to be the first that corresponds to naturally occurring atmospheric vortices. The numerical results provide strong evidence connecting the occurrence of breakdown in a tornado-like vortex jet with the non-existence of a self-similar flow to serve as the terminal state. For a non-dimensional flow force $M \equiv J/K^2 = 4$ slightly greater than the critical value M^* that prohibits similarity solutions, calculations were carried out to a height sufficient to permit very close agreement with the first-order perturbation of the corresponding self-similar flow, thus ruling out breakdown for this case. For M slightly less than the critical value M^*, vortex breakdown occurs quickly. In that case, the pressure and inertial forces were shown to dominate strongly over the viscous forces in the vicinity of the breakdown point, across the whole vortex jet. Outside a central core, the flow develops an even simpler structure in which the streamlines are merely displaced outwards by the strongly decelerating flow near the axis.

The physical relevance of this work must be assessed because of the idealizations that have been introduced to make the analysis manageable. Of these, we mention the assumptions of incompressible, laminar, steady, axisymmetric motion of a homogeneous fluid. Compressibility effects seem unimportant since recent estimates yield a maximum flow speed in tornadoes of the order of 60 m/s, much below the speed of sound. The flow in a tornado is clearly turbulent, so that a laminar analysis is equivalent to the assumption of constant eddy viscosity. Much more complicated turbulence models are now in use, but it would be rash to assert that they can give better results

† Barcilon (1967) has presented a purely inviscid treatment of breakdown in a tornado-like vortex. Our results, on the other hand, indicate that viscous effects remain important up to the immediate vicinity of the breakdown point ($z^* = Z^* K\delta/\nu$), with only the final approach to breakdown governed by inviscid processes.

in the present case, since little is known about the turbulence structure in a tornado. Our approach has been to emphasize the process of vortex breakdown without over-complicating the flow model.

The assumption of steady axisymmetric flow rules out the multiple-vortex type of tornadoes observed in recent years; these may be a manifestation of another type of vortex breakdown. Nevertheless the single-vortex type occurs in large numbers and appears to be well suited to this type of representation. Finally, it is our belief that the assumption of a homogeneous fluid is justified on the basis that gradients of flow properties are very large near breakdown. Hence the length scale over which vortex breakdown occurs is small compared with that which would be needed by any driving force due to moisture content.

The boundary condition on axial velocity, namely that $w \sim K/2\frac{1}{2}r$ as $r \to \infty$, implies that the flow outside the viscous core contains vorticity. Such a distribution of vorticity might be produced by baroclinic processes. There is no clear evidence from available tornado data that either supports or refutes such a contention.

As a qualitative test of physical relevance, we have compared the results of our calculations with observations of the 1957 Dallas tornado.† Hoecker (1960) gives the maximum vertical velocity as about 230 ft/s at a height of 150 ft above the ground. At this height the peak swirl velocity is about 190 ft/s at a radius of 120 ft from the axis of symmetry, giving $K = 23\,000\,\text{ft}^2/\text{s}$. Thus $w_0\,\delta/K$ is estimated to be very nearly 1·2 ($M = 1{\cdot}7$), the value used in our breakdown calculations. From Hoecker's data, we determine the spreading rate dr/dz of the tornado core to be 0·08, based on locating the core 'edge' at the point of maximum azimuthal speed. A similar determination of the spreading rate from the numerical solution with $M = 1{\cdot}7$ (case 2 of § 4) yields $dr/dz = 8\nu/K$. Equating these gives

$$K/\nu = 100, \tag{5.1}$$

which is a Reynolds number for the tornado. Comparing altitude in the Dallas tornado with our numerical solution is difficult because the initial condition (1.11) used herein was not observed at any height in the tornado. If we equate the altitudes at which the axial velocity defect first develops in Hoecker's observations (150 ft) and in our numerical solution ($Z = 0{\cdot}138$), we have

$$z - 150 = (K\delta/\nu)(Z - 0{\cdot}138). \tag{5.2}$$

Now K/ν is given in (5.1) and δ is 120 ft as stated above, so substitution into (5.2) with $Z^* = 0{\cdot}202$ yields $z^* = 920$ ft as the predicted location of the beginning of flow reversal (vortex breakdown), as compared with an observed value of 850 ft from Hoecker (1960). Unfortunately, the magnitudes of the axial velocity at altitudes below the breakdown location do not compare well with our results, so that the close agreement above on breakdown height should be regarded with reservation.

The authors wish to thank Mr Karl Rust for his technical assistance. The work reported herein was sponsored by the National Severe Storms Laboratory (U.S Department of Commerce, National Oceanic and Atmospheric Administration).

† Hoecker's data analysis has been criticized as inaccurate, but it is better than anything else available at this time.

REFERENCES

BARCILON, A. 1967 Vortex decay above a stationary boundary. *J. Fluid Mech.* **27**, 155.

BENJAMIN, T. B. 1967 Some developments in the theory of vortex breakdown. *J. Fluid Mech.* **28**, 65.

BURGGRAF, O. R. & FOSTER, M. R. 1975 Theoretical study of vortex breakdown in tornado-like vortices. *Final Rep. U.S. Dept. Commerce*, grant 04-3-022-37.

BURGGRAF, O. R., STEWARTSON, K. & BELCHER, R. 1971 The boundary layer induced by a potential vortex. *Phys. Fluids* **14**, 1921.

HALL, M. G. 1966 The structure of concentrated vortex cores. *Prog. Aero. Sci.*, vol. **7**. Pergamon.

HALL, M. G. 1967 A numerical method of solving the equations of the vortex core. *Aero. Res. Counc. R. & M.* no. 3467.

HALL, M. G. 1972 Vortex breakdown. *Ann. Rev. Fluid Mech.* **4**, 195.

HARVEY, J. K. 1962 Some observations of the vortex breakdown phenomenon. *J. Fluid Mech.* **14**, 585.

HOECKER, W. H. 1960 Wind speed and air flow patterns in the Dallas tornado of April 2, 1957. *Mon. Weather Rev.* **88**, 167.

KIRKPATRICK, D. L. I. 1964 Experimental investigation of the breakdown of a vortex in a tube. *R.A.E. Tech. Note* Aero 2963, ARC 26227.

LAMBOURNE, N. C. & BRYER, D. W. 1961 The bursting of leading-edge vortices – some observations and discussion of the phenomenon. *Aero. Res. Counc. R. & M.* no. 3282.

LONG, R. R. 1962 A vortex in an infinite viscous fluid. *J. Fluid Mech.* **11**, 611.

MAGER, A. 1972 Dissipation and breakdown of a wing-tip vortex. *J. Fluid Mech.* **55**, 609.

MORTON, B. R. 1969 The strength of vortex and swirling core flows. *J. Fluid Mech.* **38**, 315.

NACHTSHEIM, P. R. & SWIGERT, P. 1965 Satisfaction of asymptotic boundary conditions in numerical solution of systems of non-linear equations of boundary layer type. *N.A.S.A. Tech. Note* D-3004.

RANDALL, J. D. & LEIBOVICH, S. 1973 The critical state: a trapped wave model of vortex breakdown. *J. Fluid Mech.* **58**, 495.

REBER, C. M. 1954 The South Platte Valley tornadoes of June 7, 1953. *Bull. Am. Met. Soc.* **35**, 191.

SARPKAYA, T. 1971 On stationary and travelling vortex breakdowns. *J. Fluid Mech.* **45**, 545.

SQUIRE, H. B. 1960 Analysis of the 'vortex breakdown' phenomenon. Part I. *Imp. Coll. Aero. Dept. Rep.* no. 102.

WARD, N. B. 1972 The explanation of certain features of tornado dynamics using a laboratory model. *J. Atmos. Sci.* **29**, 1194.

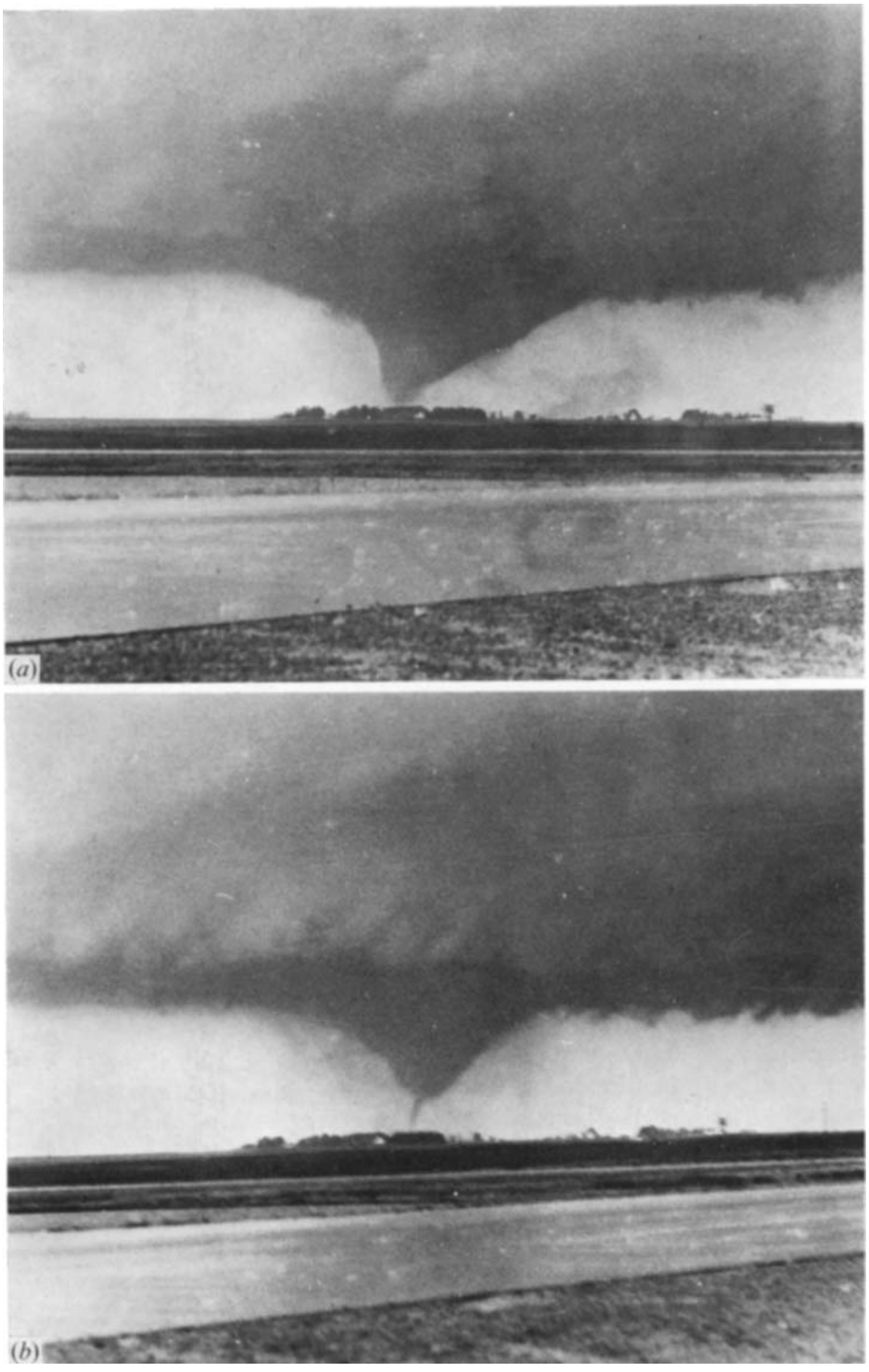

PLATE 1. Photographs of the Jordon, Iowa tornado 13 June 1976. (*a*) The tornado with a nearly conical funnel. (*b*) The tornado a short time later with the bulge on the visible core. The tornado later reassumed the form shown in (*a*), followed once more by the appearance of the bulge midway up the core. (Photographs by Jim Bruzek, courtesy NSSL.)